IEEE Access
Multidisciplinary | Rapid Review | Open Access Journal

Received March 14, 2020, accepted March 22, 2020, date of publication March 26, 2020, date of current version April 14, 2020.

Digital Object Identifier 10.1109/ACCESS.2020.2983482

A Meta-Surface Antenna Array Decoupling (MAAD) Design to Improve the Isolation Performance in a MIMO System

ZIYANG WANG[1], (Member, IEEE), CHENGLEI LI[1], (Student Member, IEEE), AND YINGZENG YIN[2], (Member, IEEE)

[1]Beijing National Research Center for Information Science and Technology, Department of Electronic Engineering, Tsinghua University, Beijing 100084, China
[2]National Key Laboratory of Antennas and Microwave Technology, Xidian University, Xi'an 710071, China

Corresponding author: Ziyang Wang (wangziyang1@tsinghua.edu.cn)

This work was supported by the China Postdoctoral Science Foundation under Grant 2019M650677.

ABSTRACT In this paper, a design to reduce the mutual coupling between two closely MIMO antennas is presented. A metasurface superstrate consisting of periodic circular split ring resonator (CSRR) elements is placed above the coupled two-element patch antennas to improve the isolation performance. The propagation of the electromagnetic wave from antenna 1 to antenna 2 causing mutual coupling will be blocked since the loading of metasurface, which can be considered as a negative-permeability medium. First, the size of the CSRR element is determined by properly designing the range of negative permeability in the desire band. Thereafter, a decoupled MIMO array with a high isolation performance is realized with an intolerable matching curve. Then, some measures are employed on each patch to enhance the matching performance, such as etching slots and loading short probes on the patches. Next, two prototypes for the coupled and decoupled arrays are fabricated and measured to verify the improvement of the isolation performance. Measured results show that the value of |S21| for the decoupled array has been greatly improved from −8 dB to less than −20 dB within the entire working band of 5.58-6.0 GHz. Meanwhile, the match bandwidth of |S11| < −15 dB for the decoupled array is approximately 420 MHz, which has also been improved in the desire band compared with the coupled array. In addition, the measured gains for the decoupled array are improved by approximately 1.8 dB as compared to the coupled array, whereas the efficiencies are increased by 16% which is higher than the coupled array. Moreover, the envelope correlation coefficient (ECC) for the decoupled array is reduced from 0.17 to 0.06 within the entire band of interest. Therefore, all measured results demonstrate that the proposed MAAD design is a good candidate for the improvement of MIMO antenna arrays.

INDEX TERMS MIMO, metasurface antenna array decoupling (MAAD), split ring resonators (SRRs).

I. INTRODUCTION

There is unprecedented growth in the demand for high data rates and wide spectrum resources for wireless communication, especially the fifth generation mobile communication [1], which has greatly promoted the development of wireless technologies and mobile electronic devices. It is both an opportunity and a challenge for antenna designers. In recent years, several advanced technologies were emerged for the design of antennas and arrays, such as MIMO array, massive MIMO, millimeter wave and full-duplex. The multiple-input multiple-output (MIMO) technology provides an effective method by using multiple paths to enhance the data throughput [2]. Therefore, MIMO/Massive MIMO, acting as a core technology of wireless communication, has attracted widespread attention for the enhancement of the spectrum efficiency and data rate of transmission. However, a practical MIMO antenna array must be compact because of limited space to satisfy the demand for antenna wide band miniaturization in either a mobile terminal or a base station. That is to say, the distance between two adjacent antenna elements is very short approximately a fraction of

The associate editor coordinating the review of this manuscript and approving it for publication was Chan Hwang See.

the wavelength in a vacuum. Hence, strong mutual coupling occurs and drastically increases with the decreasing of the distance between the two closely elements. Meanwhile, the performance of the MIMO antenna array will rapidly deteriorate in terms of the side-lobes [3], [4], efficiencies [5], the envelop correlation [6], [7] and signal-to-noise ratio [5]. Channel capacity for the MIMO system will also be greatly reduced since of mutual coupling. Therefore, it is necessary to study the array coupling reduction technology used in MIMO antenna systems.

Currently, many articles on the decoupling design of MIMO antenna are reported, which can be divided into the following categories.

(1) Ground modification design: By loading branch structures or etching defected ground structures (DGS) on the ground plane, the induced current that causes the mutual coupling decreases, and the common ground is modified.

The published methods also vary and describe methods involving etching of S-shaped periodic structure [8], embedding of tree-shape structure [9] and insertion of T-shaped branches.

(2) Neutralization line design: Connected lines with different shapes [10], [11] are introduced between two antennas to cancel out the reactive coupling. This has been used in practical applications for mobile phone antenna. In addition, relevant reports can be extended to single-frequency WLAN [12], dual bands [13] and UWB antenna [14].

(3) Parasitic element design: A coupled or parasitic structure [15] is loaded between two antennas [16]. Hence, the structure is not connected with the radiation antenna and the ground [17].

(4) Network decoupling technology: The coupling between two antennas is greatly reduced by circuit theory. Examples include the characteristic modes [18], multi-ports conjugate (MC) match [19] as well as coupling resonator decoupling network (CRDN) [20], [21]. CRDN as a decoupling method first appeared in mobile terminals [20]; subsequently, a dual band CRDN decoupling technology was also presented in [21].

Because of its novel electromagnetic characteristics, artificial electromagnet material has become a hot academic research topic for which novel electromagnetic phenomena have been discovered [22]. In particular, the emergence of the metasurface has greatly promoted the development of electromagnetic materials. Various new electromagnetic devices and microwave applications have been developed. For example, for the production of high gains, Fabry-Perot cavity antennas, reflectarray antennas [23] and transmitarray antennas [24] are proposed; for the reduction of the radar cross section (RCS) [25], the low-RCS antenna is realized; for the modulation of polarization, polar covers and OAM antennas [26] are presented. In addition, the metamaterial-based or metasurface can also be utilized for decoupling in MIMO antennas array.

Based on the working mechanism of decoupling with metamaterials, this decoupling methods can be divided into three types as follows:

a) Electromagnetic band gap (EBG) and waveguide metamaterials: these can inhibit the surface wave to some extent. Waveguide metamaterials have been designed and presented [27], [28]. In addition, the EBG structure can be used to decouple the array antennas in [29]. Moreover, many deformed structures of EBG are presented, such as a two-layer EBG structure [30], a tunable EBG using the biasing technique, as well as the combination of the action of EBG and SRRs [31] to improve the isolation. Furthermore, EBG for decoupling can be applied in UWB antennas [32] and even millimeter wave fields [33].
b) Meta-cloak and metamaterial insulators: some measures have been adapted to reduce the near-field coupling. In [34], metamaterial EM insulator technology is introduced to reduce the antenna coupling in the E-plane, which has been realized in a five-element array. In [35], a metamaterial isolation wall is utilized between two dielectric resonator antennas (DRAs) for decoupling at 60 GHz. This type of decoupling method has been realized in terahertz (THz) applications using graphene metasurfaces [36].
c) Metasurface decoupling design: a certain decoupling space is required between two coupled antennas by using the two metamaterial-based methods mentioned above. To compensate for the shortcomings of the small space in a compact array, the proposed metasurface decoupling technology emerged. Moreover, the used of an array-antenna decoupling surface for the improvement of isolation is first presented in two practical examples [37]. Then, a modified array decoupling surface is utilized for the decoupling of a dual band antenna [38]. Next, an EBG surface [39] is adapted as a ground for decoupling in the millimeter wave band which is different from the metasurface.

In this paper, a design for metasurface array antenna decoupling (MAAD) is presented for a compact coupled two-element array. The proposed decoupling method has the following advantages. First, the isolation performance and bandwidth for the decoupled antenna array have been significantly improved than before. Next, the space between the two elements is less than 0.02 wavelength which is quite compact comparing with other published papers. Then, the radiation performances in far-field, such as gains, efficiencies and ECC, have also been greatly improved. In addition, it is easily expanded for use in massive MIMO arrays, which have hundreds of cells. The theory and analysis for decoupling are developed in Section II, and the results of measurements and simulations are presented in Section III. Finally, a summary is given in section IV.

II. ANTENNA DESIGN AND ANALYSIS

A. METAMATERIAL UNIT

A network theory model for an isotropic homogenous material is used to compute the permittivity and permeability of the

proposed metamaterial element. Then, the composite terms V_1 and V_2 are introduced to compute the effective permittivity ε_r and the effective permeability μ_r of the medium by using the following formulas (1-5).

$$V_1 = S_{21} + S_{11} \tag{1}$$
$$V_2 = S_{21} - S_{11} \tag{2}$$
$$k_0 = w/c \tag{3}$$
$$\mu_r \approx \frac{2}{jk_0 d}\frac{1 - V_2}{1 + V_2} \tag{4}$$
$$\varepsilon_r \approx \frac{2}{jk_0 d}\frac{1 - V_1}{1 + V_1} \tag{5}$$

B. DECOUPLING PRINCIPLE FOR A NEGATIVE PERMEABLITY MEDIUM

Let us consider a metasurface consisting of CSSR elements as shown in Fig. 1 (a). The effective permeability frequency bands of the CSSR cells are determined by the physical dimensions, especially the size of the ring, as shown in Fig. 1 (b). A desirable effective negative permeability region is realized by modifying the element size. To analyze the decoupling mechanism of the proposed method, a coupled two-element array is utilized as shown in Fig. 2. The undesired coupled component A_0e^{jkx} will be introduced to antenna 2 from antenna 1 with antenna 1 in an excited state, while the waves propagate along the minus X-direction. Then, a metasurface is placed above the coupled array. Let's analyze the following four cases corresponding to different characteristics of the loading metasurface in detail based on the formula (6).

$$k = w\sqrt{\mu\varepsilon} \tag{6}$$

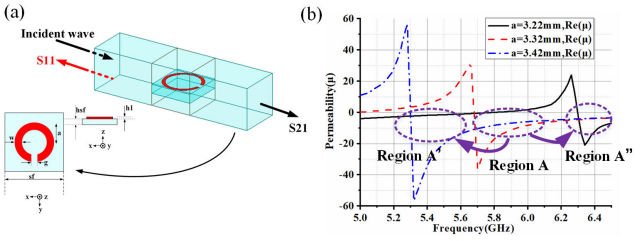

FIGURE 1. Layout of the SRRs elements, (b) the frequency response of effective permeability corresponding to different element sizes.

TABLE 1. Optimized geometric parameters for the proposed element.

Par.	Value	Par.	Val.	Par.	Val.
a	3.32	g	0.5	h1	0.035
w	0.5	sf	7	hsf	1.5

Case 1: when $\mu_r>0$, $\varepsilon_r>0$; k is a real number ($k>0$) according to formula (7), such as is observed in a conventional medium plane. The coupled energy can be calculated by formula (8). As shown in formula (8), the undesired coupled antenna will propagate along the minus X-direction as time goes on. Therefore, the mutual coupling cannot be reduced by the metasurface of this features.

$$k = w\sqrt{\mu_r\varepsilon_r\mu_0\varepsilon_0} = k_0\sqrt{|\mu_r||\varepsilon_r|} \tag{7}$$
$$A_0e^{jkx}e^{jwt} = A_0e^{j(k_0\sqrt{|\mu_r||\varepsilon_r|})x}e^{jwt} \tag{8}$$

Case 2: when $\mu_r>0$, $\varepsilon_r<0$; k is a complex number, which can be calculated with formula (9), such as in the case of negative permittivity materials (NPM) with an effective negative permittivity. Moreover, the energy that causes the coupling can also be calculated based on formula (10). The undesired coupled energy becomes a huge attenuation component due to the use of the medium for effective negative permittivity. Furthermore, the coupled energy will be greatly reduced as the distance increases in the X-direction according to formula (10). Consequently, the propagation of the electromagnetic wave coupling to the adjacent element will be rejected by using the proposed metasurface of this characteristic.

$$k = w\sqrt{\mu_r\varepsilon_r\mu_0\varepsilon_0} = jk_0\sqrt{|\mu_r||\varepsilon_r|} \tag{9}$$
$$A_0e^{jkx}e^{jwt} = A_0e^{j(jk_0\sqrt{|\mu_r||\varepsilon_r|})x}e^{jwt} = A_0e^{-(k_0\sqrt{|\mu_r||\varepsilon_r|})x}e^{jwt} \tag{10}$$

Case 3: when $\mu_r<0$, $\varepsilon_r>0$; k is a complex number, which can be computed with formula (9), such as in the case of negative magnetic permeability materials (NMPM) with the characteristic of effective negative permeability. The coupling energy also becomes an attenuation component with the increasing of distance in X-direction, which is identical to case 2. Therefore, the electromagnetic wave coupling to antenna 2 from antenna 1 also can't be propagated because of this novel feature.

Case 4: when $\mu_r<0$, $\varepsilon_r<0$; k is a real number ($k>0$), such as the case of a double negative index (DNG) medium. The analysis method is identical to that presented in case 1. The electromagnetic wave will transmit to antenna 2 from antenna 1 and cause strong mutual coupling; therefore, the coupling can't be reduced by using the metasurface with this characteristic.

Overall, the propagation of the electromagnetic wave causing the coupling will be suppressed by covering a single negative metasurface of effective permittivity or permeability. In this paper, a metasurface superstrate is introduced with an effective negative permeability in a certain frequency band for decoupling as shown in Fig. 1 (b), which can be analyzed based on case 3. In addition, it is understandable that the reflected waves from the metasurface mitigate the mutual coupling energy to improve the isolation performance of array.

C. TWO-ELEMENT ANTENNA ARRAY WITH A META-SURFACE COVERING

The geometries of the proposed MIMO antenna pair without/with a metasurface are shown in Fig. 2 and Fig. 3, respectively. As shown in Fig. 2, the coupled antenna pair is fabricated and printed on the FR4 substrate with a dielectric contains of 4.4, a loss tangent of 0.02 and a thickness of 3 mm.

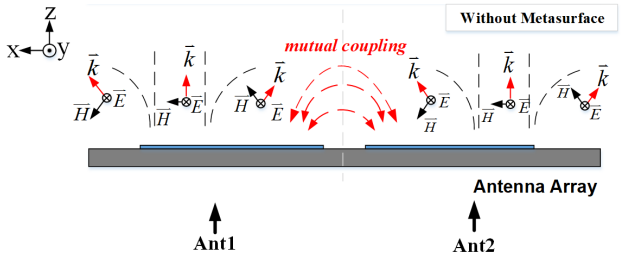

FIGURE 2. Structure diagram of a strongly coupled two-element array without a metasurface.

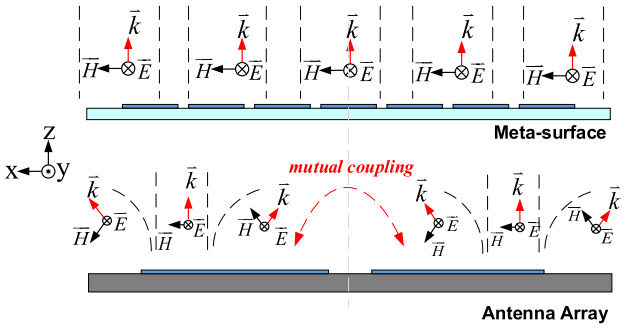

FIGURE 3. Principle of the decoupled array with a metasurface.

However, the isolation performance of this coupled MIMO antennas pair is poor which will seriously affect its radiation performance. Then, a metasurface consisting of CSRRs with a certain characteristic is placed above the coupled antenna pair. Thereafter, the isolation performance for the coupled MIMO antenna has been improved by a large margin. Next, some matching measures are introduced into the design of the decoupling MIMO antenna. Via simulation with the commercial software HFSS 16, the proposed decoupled MIMO array is optimized and designed. The detailed dimensions of this decoupled MIMO antenna are listed in Table. 2.

TABLE 2. Optimized parameters for the proposed decoupled array.

Parameters	Values	Par.	Val.	Par.	Val.
ws	40	h2	3.3	l2	5.5
ls	26	r1	0.65	lw	0.5
hs	3	r2	1.5	r3	1
wp	12.4	rp	0.5	ra	3.36
lp	12.5	p1	4	rw	0.5
ad	1	p2	0.8	rg	0.5
fy	3.3	l1	2	sf	7
hsf	1.5	unit	mm	-	-

1) DESIGN SCHEME OF THE PROPOSED DECOUPLED ANTENNA

To further explore the realization of the decoupled array, the design of scheme is presented. The structure of the coupled two-element array named Array 1 is shown in Fig. 4 (a). The strong coupling between the two antennas emerges, since the distance between the two elements is 1 mm, which is approximately 0.02 λ at the working frequency of 5.8 GHz.

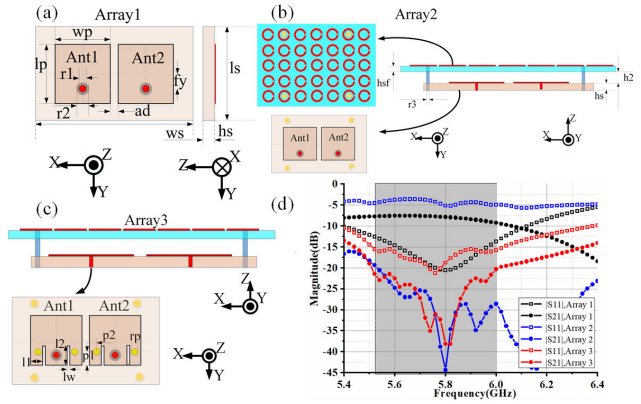

FIGURE 4. (a) Top view (left) and side view (right) for Array 1; (b) Top view (left) and side view (right) for Array 2; (c) Top view (left) and side view (right) for Array 3; (d) Simulated S-parameters of Array 1, Array 2 and Array 3.

The corresponding S parameter values of both |S11| and |S21| are shown in Fig. 4 (d). The value of |S11| is acceptable in the working frequency band, while that of |S21| is intolerable. In other words, the ability of the MIMO antennas to separately receive or transmit is seriously affected. Based on the above requirements, a metasurface with an effective negative permeability is placed above the coupled MIMO array named Array 2, as shown in Fig. 4 (b). In addition, the values of the corresponding S-parameter are presented in Fig. 4 (d). The isolation of Array 2 is greatly improved, while the matching of Array 2 cannot be tolerated. Thereafter, etching slot and loading probe technologies are both used to improve the matching as shown in Fig. 4 (c), which shows Array 3. It is exciting that both the matching and isolation performance of Array 3 can satisfy our requirements for the desired bands for the MIMO antenna.

2) DESIGN SCHEME OF MATCHING FOR THE DECOUPLED ARRAY

To analyze the matching process of Array 3 in detail, the matching techniques used for the loading probe and grooving are separately studied. In Fig. 5, different values of the S parameters for the three arrays are presented. For the first array (Array 2) with a decoupling metasurface, the isolation performance is perfect, but the matching performance is unavailable because there is no matching measure. Thereafter, two short pins are loaded in both patch antennas. As shown by the red lines in Fig. 5, the matching performance of Array 2' has been improved, meanwhile the isolation performance is not significantly attenuated. For Array 2', the matching bandwidth is narrow, especially it is poor in the high-frequency band. Next, a pair of rectangular grooves are etched on the two decoupled patch antennas, which causes to a great improvement for the matching performance in the desired band of 5.57-5.98 GHz with |S11| less than -15 dB. Moreover, there is almost no change on the isolation curve. Therefore, the metasurface-based antenna array with high performance has been realized.

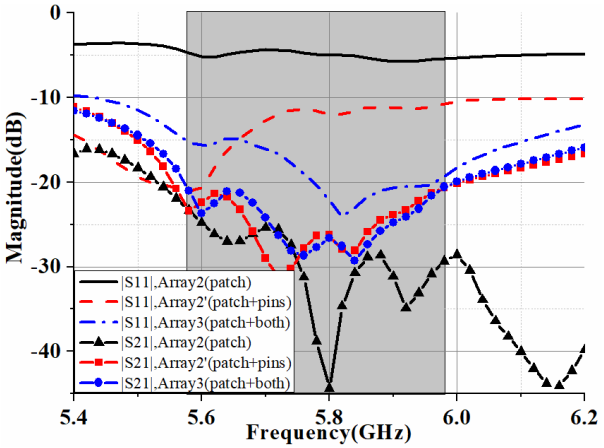

FIGURE 5. Different metasurface arrays for (a) decoupled metasurface Array 2 without matching measures, (b) decoupled metasurface Array 2′ with two short pins, and (c) decoupled metasurface Array 3 with two short pins and two rectangular grooves.

D. PARAMETRIC STUDIES

To investigate the working principle of the proposed metasurface antenna, especially the decoupling mechanism, all aspects of the MIMO array are discussed in detail as follows.

1) RESEARCH ON EFFECTS OF CSRRs ON ISOLATION

To study the effect of CSRRs on the isolation performance of the decoupled array, important parameters have been investigated for the following aspects: the size of the circular rings, size of the gap on the ring, rotation angle of the split and the height of the surface. As shown in Fig. 6, the simulated S parameter values of |S11| and |S21| are presented for different lengths of the circular rings, which is represented by "a". When the lengths of the circular rings decrease, the isolation band will shift to the high-frequency band, since the negative permeability bandwidth range of the proposed CSRR elements is shifted to a high frequency. It logically shifts to a low frequency with the increasing to the size of the circular rings. The matching bandwidth with the changing of

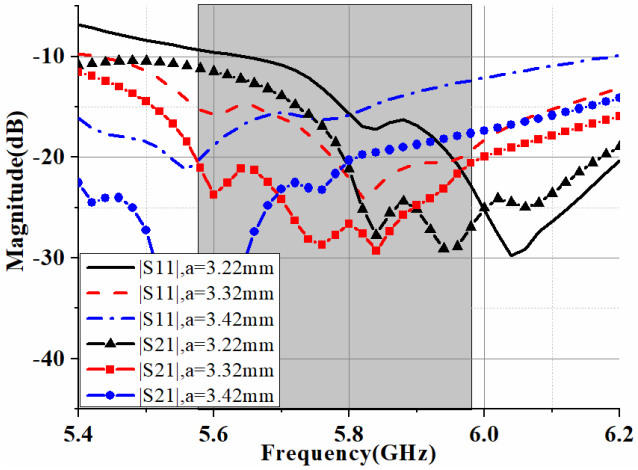

FIGURE 6. Simulated S parameter of Array 3 with different a values.

the circular ring is also affected to some extent. In addition, the performance of isolation and matching will be affected by the gap in the ring as shown in Fig. 7. When the gap becomes large, the resonant frequency of |S11| and |S21| shifts to high frequency as shown in Fig. 7. Otherwise, it moves to low frequency in Fig. 7. Then, the rotation angle of the CSRRs is also investigated in this section, while the response curves for matching and isolation show almost no change when the range of the rotation angle covers 20° from -10° to 10°, as shown in Fig. 8. Generally, there is no significant change in the equivalent length with the changing of the rotation angle. Next, the height of the proposed surface as a key parameter is also investigated, and the performance regularly changes as shown in Fig. 9. The performance of the antenna with a high profile will be better than a low one, but a surface placing at a high position will increase the size of the proposed metasurface MIMO antenna array.

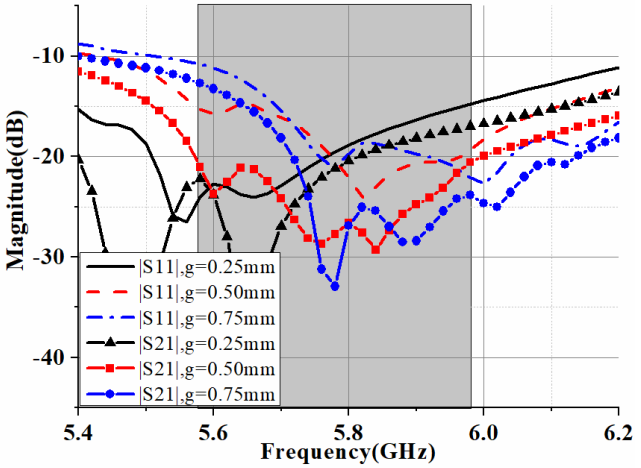

FIGURE 7. Simulated S parameter of Array 3 with different g values.

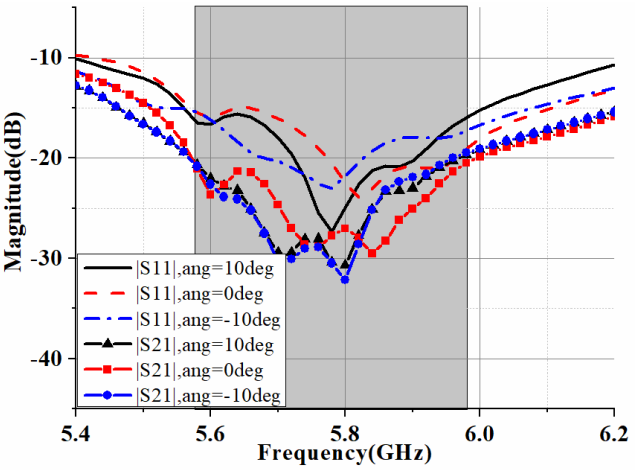

FIGURE 8. Simulated S parameter of Array 3 with different ang values.

2) RESEARCH OF MATCHING CHARACTERISTICS

For the matching characteristics, the key parameters are also analyzed in detail, such as the lengths of the slot lines and the positions of the probes. As shown in Fig. 10, the length of

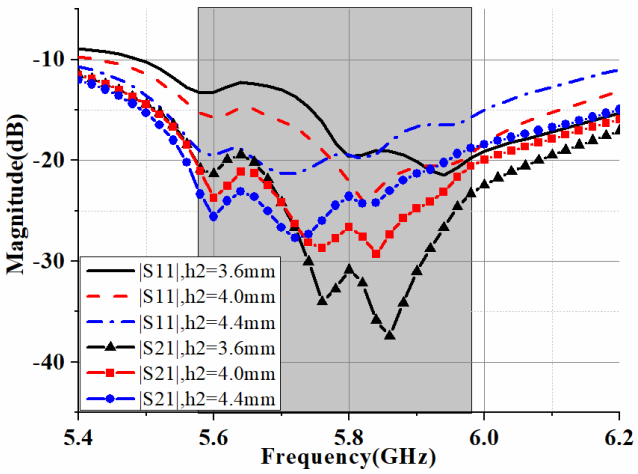

FIGURE 9. Simulated S parameter of Array 3 with different h2 values.

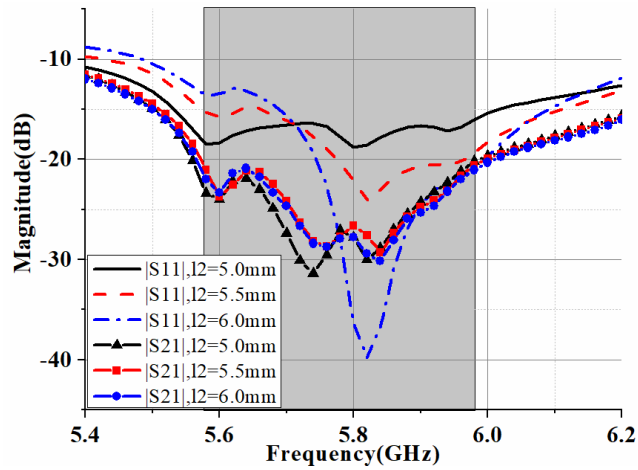

FIGURE 10. Simulated S parameter of Array 3 with different values of l2.

two slot lines, which is represented by "l2", are investigated. Moreover, the high-frequency resonance point of |S11| is subject to violent fluctuation, while the low frequency resonance point has a small change. Meanwhile, the isolation curves have no change in the working frequency band, although the length of the slot line changes from 5.0 mm to 6.0 mm. Next, the position of the two probes is analyzed as shown in Fig. 11. The impact of two probes at the high frequency band is enormous, either on the matching or isolation curves. However, there is no changing at the low frequency working band about the curves of |S21| and |S11| with the shifting of the position for two probes.

3) ANALYSIS OF THE NUMBER OF SRRS AND THE SPACING BETWEEN TWO ELEMENTS

In Fig. 12, the number of CSRR elements for increasing matching and isolation performance are investigated in Fig. 12. It is clear that the set of 5 × 7 CSRR units has a better performance than the others sets.

Moreover, to quantify the effectiveness of the proposed decoupling method using a metasurface cover, the isolation

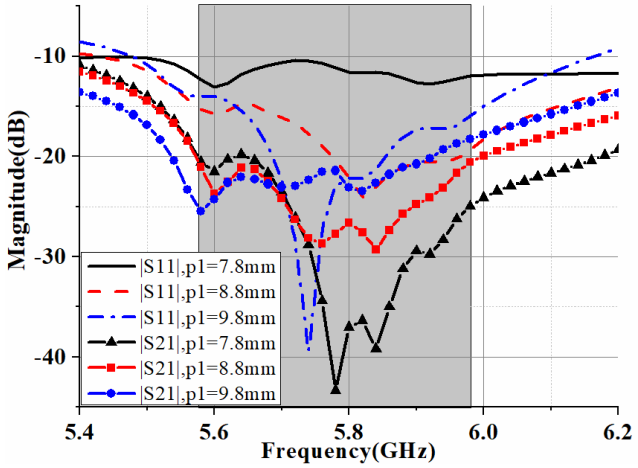

FIGURE 11. Simulated S parameter of Array 3 with different values of p1.

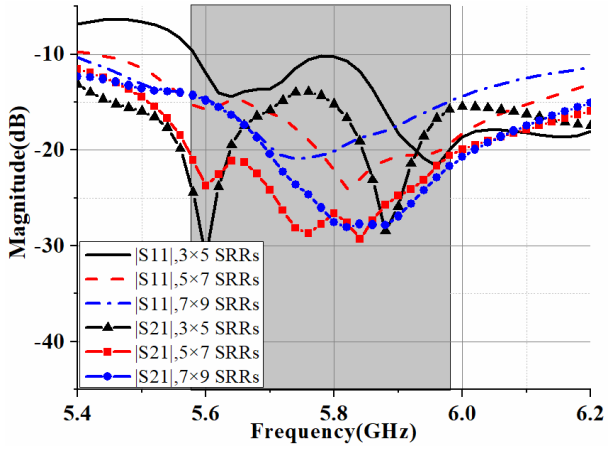

FIGURE 12. Simulated S parameter of Array 3 with different CSRR numbers.

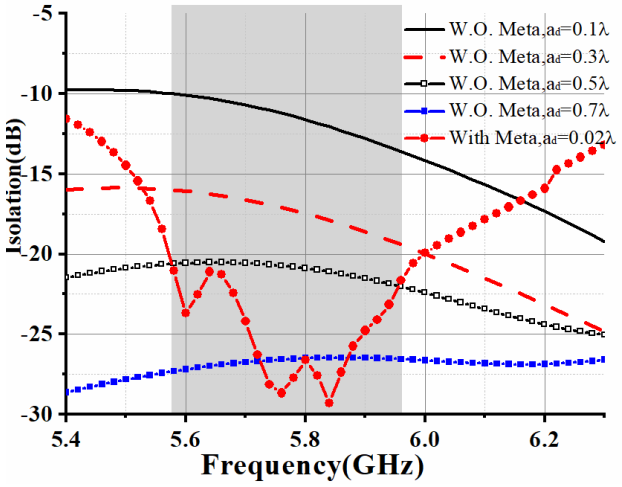

FIGURE 13. Simulated isolation curves for arrays with different values of ad comparing with the proposed MAAD technology.

between two elements with different edge-to-edge distances "ad" are analyzed. Meanwhile, the isolation curve for the decoupled array is also presented with a close unit distance approximately 0.02 λ as shown in Fig. 13. In the desired

working band, the isolation of the proposed decoupled array with a metasurface is equivalent to that of the array without a metasurface, in which the element distance is approximately 30-fold greater.

4) CURRENT DISTRIBUTIONS ON THE SURFACE OF TWO PATCHES

As shown in Fig. 14, the current distributions on the two patches with and without a metasurface are presented, respectively. The coupled currents on the array without a metasurface are obvious when antenna 1 is excited. However, the coupled currents on antenna 2 have been greatly decreased on the decoupled array with a metasurface, as shown in Fig. 14 (b). Therefore, the metasurface decoupling method is effective for antennas array.

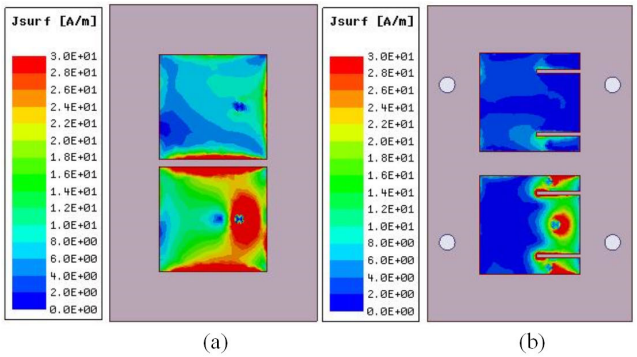

FIGURE 14. Surface current distributions for the two arrays (a) with and (b) without a metasurface when antenna 1 is excited.

III. RESULTS AND ANALYSIS

A. S-PARAMETERS

To verify the effects of the loaded and unloaded decoupled metasurface, both Array 1 and Array 3 are manufactured and measured. And the prototypes for coupled and decoupled array are shown in Figs. 15 and 16, respectively. Then, the S parameters for two arrays are tested by using Keysight E5080A vector network analyzer. Moreover, the simulated and measured data for the coupled and decoupled array are presented in Figs. 15 and 16. It is obvious that the mutual coupling has been greatly reduced by more than 20 dB in the desired band of 5.58-6.0 GHz. Furthermore, the test data are highly consistent with simulation data.

B. RADIATION PARAMETERS

The co-polar and cross-polar 2D patterns for the coupled and decoupled arrays with antenna 1 in an excited state in different planes are presented in Fig. 17. The values of the patterns in the XOZ plane are shown in Fig. 17 (a), and those setting in the YOZ plane are in presented Fig. 17 (b). Next, the data for antenna 2 excited are shown in Figs. 17 (c) and (d). Then, measured peak gains and efficiencies for the coupled and decoupled arrays at different frequencies are presented in Figs. 17 (e) and (f), respectively. The gains for the decoupled antenna have been improved by approximately 1.8 dB compared to those of the coupled antenna. Meanwhile,

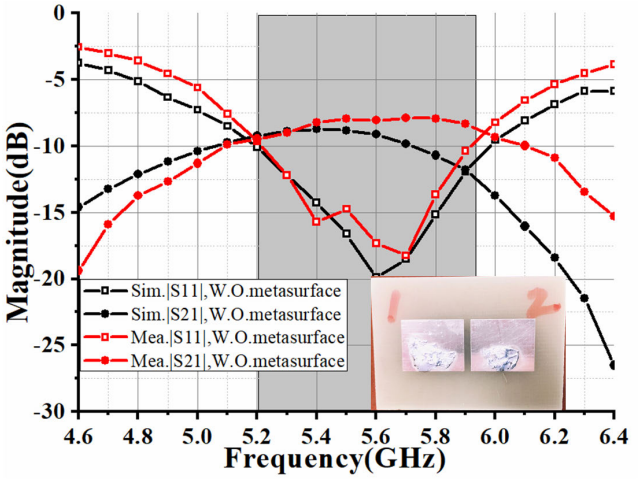

FIGURE 15. Simulated and measured S parameter of Array 1 without a metasurface.

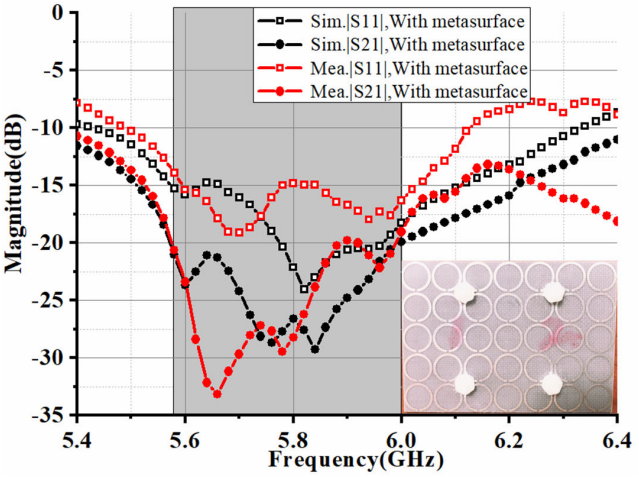

FIGURE 16. Simulated and measured S parameter of Array 3 with the metasurface.

TABLE 3. Comparisons of the proposed method with referenced antennas.

Ref.	Method	Freq	|S21|	E-E(λ_0)	Height (λ_0)
[8]	DGS	2.57	41	0.22	0.03
[11]	Neutral.	5.8	19.6	0.18	N/A
[15]	Parasitic	2.45	30	0.08	0.02
[29]	EBG	5.86	-24	0.75	0.04
[35]	Cloak	60	-30	0.5	0.3
Pro.	MAAD	5.8	-20	0.02	0.12

Notes: "Freq" is the abbreviation of "Frequency" with the unit of GHz; "|S21|" is the value of isolation with the unit of dB; "E-E" is the abbreviation of "edge to edge"; and λ_0 is the wavelength in vacuum; "height" is the profile of the decoupling metasurface antenna.

the efficiencies for the proposed decoupled antenna have also been enhanced by about 16 % in the desired bands.

C. ENVELOPE CORRELATION COEFFIEICENT (ECC)

The envelope correlation coefficient (ECC) as an important indicator for MIMO systems is also investigated. The value of ECC can be obtained with Formula. 11. $\vec{E_i}(\theta, \phi)$ is the

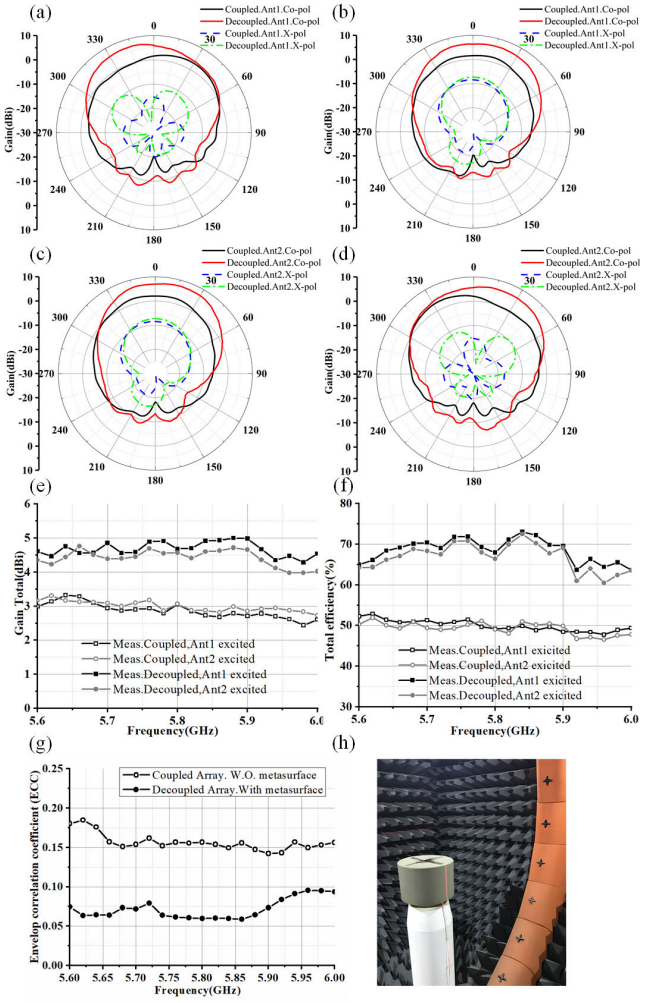

FIGURE 17. (a) 2D radiation patterns of co-polar and cross-polar for coupled and decoupled arrays with antenna 1 excited in XOZ plane, (b) 2D radiation patterns of co-polar and cross-polar for coupled and decoupled arrays with antenna 1 excited in YOZ plane, (c) 2D radiation patterns of co-polar and cross-polar for coupled and decoupled arrays with antenna 2 excited in XOZ plane, (d) 2D radiation patterns of co-polar and cross-polar for coupled and decoupled arrays with antenna 2 excited in YOZ plane, (e) measured peak gains of the coupled and decoupled arrays with respects to different frequencies, (f) measured total efficiencies of the coupled and decoupled arrays with respects to different frequencies, (g) measured values of ECC for the arrays with and without metasurface, (h) test environment.

measured electric field vector radiated by antenna i, while another port is terminated by 50 Ω. Then, the calculated ECCs for the arrays with and without a metasurface are given in Fig. 17 (g). It is obvious that the ECC has been improved from 0.18 to less than 0.07 by using the proposed MAAD method.

$$\rho_e = \frac{\left| \iint_{4\pi} [\vec{E_1}(\theta,\phi) \cdot \vec{E_2}(\theta,\phi)] d\Omega \right|^2}{\iint_{4\pi} |\vec{E_1}(\theta,\phi)|^2 d\Omega \iint_{4\pi} |\vec{E_2}(\theta,\phi)|^2 d\Omega} \tag{11}$$

$$\vec{E_1}(\theta,\phi) \cdot \vec{E_2}(\theta,\phi) = \vec{E}_{\theta 1}(\theta,\phi) \vec{E}^*_{\theta 2}(\theta,\phi) + \vec{E}_{\phi 1}(\theta,\phi) \vec{E}^*_{\phi 2}(\theta,\phi) \tag{12}$$

D. COMPARISON WITH THE REFERENCED ANTENNA

Table 3 shows the comparisons between the proposed MAAD with other decoupling technologies, such as DGS, neutralization line, parasitic element, EBG and meta-clock. Moreover, the value of |S21|, the distance of edge-to-edge and the height of the metasurface are presented in this table. As shown in Table 3, an obvious advantage is the achievement of the decoupling in a compact space between two coupled antennas, and the profile of the proposed decoupled array is acceptable.

IV. CONCLUSION

In this paper, a metasurface antenna array decoupling (MAAD) method is proposed. Firstly, the detailed design of the CSRR element, working principle of decoupling and design process are presented. Then, some key parameters for matching and isolation performance are studied. Next, two prototypes for the coupled and decoupled arrays are fabricated and measured, test data show that the isolation performance is greatly improved from -8dB to -20dB in the entire working band of 5.58-6.0 GHz by using this proposed MAAD technology. Meanwhile, the gains for the decoupled array have been increased by approximately 1.8 dB which is higher than the coupled array, and the efficiencies have been improved about 16% compared with the coupled array. In addition, the value of ECC has also been improved from 0.17 to 0.06. Therefore, the signs suggest that the proposed MAAD technique has great potential to be used in improving the performance of MIMO antennas.

REFERENCES

[1] *Requirements for Further Advancements for Evolved Universal Terrestrial Radio Access (E-UTRA) (LTE-Advanced)*, document TR 36.913, Version 11.0.0, 3GPP, Nov. 2012.

[2] A. A. Deshmukh and K. P. Ray, "Broadband proximity-fed modified rectangular microstrip antennas," *IEEE Antennas Propag. Mag.*, vol. 53, no. 5, pp. 41–56, Oct. 2011.

[3] H. Steyskal and J. S. Herd, "Mutual coupling compensation in small array antennas," *IEEE Trans. Antennas Propag.*, vol. 38, no. 12, pp. 1971–1975, Dec. 1990.

[4] D. Pozar, "Considerations for millimeter wave printed antennas," *IEEE Trans. Antennas Propag.*, vol. AP-31, no. 5, pp. 740–747, Sep. 1983.

[5] M. A. Jensen and J. W. Wallace, "A review of antennas and propagation for MIMO wireless communications," *IEEE Trans. Antennas Propag.*, vol. 52, no. 11, pp. 2810–2824, Nov. 2004.

[6] L. Lu, G.-Y. Li, and A.-L. Swindlehurst, "An overview of massive MIMO: Benefits and challenges," *IEEE J. Sel. Topics Signal Process.*, vol. 8, no. 5, pp. 742–758, Oct. 2014.

[7] P. S. Taluja and B. L. Hughes, "Diversity limits of compact broadband multi-antenna systems," *IEEE J. Sel. Areas Commun.*, vol. 31, no. 2, pp. 326–337, Feb. 2013.

[8] K. Wei, L. Wang, Z. Xing, R. Xu, and J. Li, "S-shaped periodic defected ground structures to reduce microstrip antenna array mutual coupling," *Electron. Lett.*, vol. 52, no. 15, pp. 1288–1290, Jul. 2016.

[9] S. Zhang, Z. Ying, J. Xiong, and S. He, "Ultrawideband MIMO/diversity antennas with a tree-like structure to enhance wideband isolation," *IEEE Antennas Wireless Propag. Lett.*, vol. 8, pp. 1279–1282, 2009.

[10] C. H. See, R. A. Abd-Alhameed, Z. Z. Abidin, N. J. McEwan, and P. S. Excell, "Wideband printed MIMO/diversity monopole antenna for WiFi/WiMAX applications," *IEEE Trans. Antennas Propag.*, vol. 60, no. 4, pp. 2028–2035, Apr. 2012.

[11] H.-L. Peng, R. Tao, W.-Y. Yin, and J.-F. Mao, "A novel compact dual-band antenna array with high isolations realized using the neutralization technique," *IEEE Trans. Antennas Propag.*, vol. 61, no. 4, pp. 1956–1962, Apr. 2013.
[12] S.-W. Su, C.-T. Lee, and F.-S. Chang, "Printed MIMO-antenna system using neutralization-line technique for wireless USB-dongle applications," *IEEE Trans. Antennas Propag.*, vol. 60, no. 2, pp. 456–463, Feb. 2012.
[13] S. Wang and Z. Du, "Decoupled dual-antenna system using crossed neutralization lines for LTE/WWAN smartphone applications," *IEEE Antennas Wireless Propag. Lett.*, vol. 14, pp. 523–526, 2015.
[14] S. Zhang and G. F. Pedersen, "Mutual coupling reduction for UWB MIMO antennas with a wideband neutralization line," *IEEE Antennas Wireless Propag. Lett.*, vol. 15, pp. 166–169, 2016.
[15] Y.-F. Cheng, X. Ding, W. Shao, and B.-Z. Wang, "Reduction of mutual coupling between patch antennas using a polarization-conversion isolator," *IEEE Antennas Wireless Propag. Lett.*, vol. 16, pp. 1257–1260, 2017.
[16] A. C. K. Mak, C. R. Rowell, and R. D. Murch, "Isolation enhancement between two closely packed antennas," *IEEE Trans. Antennas Propag.*, vol. 56, no. 11, pp. 3411–3419, Nov. 2008.
[17] B. K. Lau and J. B. Andersen, "Simple and efficient decoupling of compact arrays with parasitic scatterers," *IEEE Trans. Antennas Propag.*, vol. 60, no. 2, pp. 464–472, Feb. 2012.
[18] K. Wang, L. Li, and T. F. Eibert, "Comparison of compact monopole antenna arrays with Eigenmode excitation and multiport conjugate matching," *IEEE Trans. Antennas Propag.*, vol. 61, no. 8, pp. 4054–4062, Aug. 2013.
[19] B. K. Lau, J. B. Andersen, G. Kristensson, and A. F. Molisch, "Impact of matching network on bandwidth of compact antenna arrays," *IEEE Trans. Antennas Propag.*, vol. 54, no. 11, pp. 3225–3238, Nov. 2006.
[20] L. Zhao, L. K. Yeung, and K.-L. Wu, "A coupled resonator decoupling network for two-element compact antenna arrays in mobile terminals," *IEEE Trans. Antennas Propag.*, vol. 62, no. 5, pp. 2767–2776, May 2014.
[21] L. Zhao and K.-L. Wu, "A broadband coupled resonator decoupling network for a three-element compact array," in *IEEE MTT-S Int. Microw. Symp. Dig.*, Jun. 2013, pp. 1–3.
[22] J. B. Pendry, A. J. Holden, W. J. Stewart, and I. Youngs, "Extremely low frequency plasmons in metallic mesostructures," *Phys. Rev. Lett.*, vol. 76, no. 25, pp. 4773–4776, 1996.
[23] Q. Luo, S. Gao, W. Li, M. Sobhy, I. Bakaimi, C. H. K. de Groot, B. Hayden, I. Reaney, and X. Yang, "Multibeam dual-circularly polarized reflectarray for connected and autonomous vehicles," *IEEE Trans. Veh. Technol.*, vol. 68, no. 4, pp. 3574–3585, Apr. 2019.
[24] G.-B. Wu, S.-W. Qu, and S. Yang, "Low-profile transmitarray antenna with cassegrain reflectarray feed," *IEEE Trans. Antennas Propag.*, vol. 67, no. 5, pp. 3079–3088, May 2019.
[25] Y. Liu, K. Li, Y. Jia, Y. Hao, S. Gong, and Y. J. Guo, "Wideband RCS reduction of a slot array antenna using polarization conversion metasurfaces," *IEEE Trans. Antennas Propag.*, vol. 64, no. 1, pp. 326–331, Jan. 2016.
[26] S. Yu, L. Li, and G. Shi, "Dual-polarization and dual-mode orbital angular momentum radio vortex beam generated by using reflective metasurface," *Appl. Phys. Express*, vol. 9, no. 8, pp. 082202–082206, 2016.
[27] H.-X. Xu, G.-M. Wang, and M.-Q. Qi, "Hilbert-shaped magnetic waveguided metamaterials for electromagnetic coupling reduction of microstrip antenna array," *IEEE Trans. Magn.*, vol. 49, no. 4, pp. 1526–1529, Apr. 2013.
[28] X. M. Yang, X. G. Liu, X. Y. Zhou, and T. J. Cui, "Reduction of mutual coupling between closely packed patch antennas using waveguided metamaterials," *IEEE Antennas Wireless Propag. Lett.*, vol. 11, pp. 389–391, 2012.
[29] F. Yang and Y. Rahmat-Samii, "Microstrip antennas integrated with electromagnetic band-gap (EBG) structures: A low mutual coupling design for array applications," *IEEE Trans. Antennas Propag.*, vol. 51, no. 10, pp. 2936–2946, Oct. 2003.
[30] S. Ghosh, T.-N. Tran, and T. Le-Ngoc, "Dual-layer EBG-based miniaturized multi-element antenna for MIMO systems," *IEEE Trans. Antennas Propag.*, vol. 62, no. 8, pp. 3985–3997, Aug. 2014.
[31] J.-Y. Lee, S.-H. Kim, and J.-H. Jang, "Reduction of mutual coupling in planar multiple antenna by using 1-D EBG and SRR structures," *IEEE Trans. Antennas Propag.*, vol. 63, no. 9, pp. 4194–4198, Sep. 2015.
[32] Q. Li, A. P. Feresidis, M. Mavridou, and P. S. Hall, "Miniaturized double-layer EBG structures for broadband mutual coupling reduction between UWB monopoles," *IEEE Trans. Antennas Propag.*, vol. 63, no. 3, pp. 1168–1171, Mar. 2015.
[33] R. Karimian, A. Kesavan, M. Nedil, and T. A. Denidni, "Low-mutual-coupling 60-GHz MIMO antenna system with frequency selective surface wall," *IEEE Antennas Wireless Propag. Lett.*, vol. 16, pp. 373–376, 2017.
[34] K. Buell, H. Mosallaei, and K. Sarabandi, "Metamaterial insulator enabled superdirective array," *IEEE Trans. Antennas Propag.*, vol. 55, no. 4, pp. 1074–1085, Apr. 2007.
[35] A. Dadgarpour, B. Zarghooni, B. S. Virdee, T. A. Denidni, and A. A. Kishk, "Mutual coupling reduction in dielectric resonator antennas using metasurface shield for 60-GHz MIMO systems," *IEEE Antennas Wireless Propag. Lett.*, vol. 16, pp. 477–480, 2017.
[36] J. Ghosh and D. Mitra, "Mutual coupling reduction in planar antenna by graphene metasurface for THz application," *J. Electromagn. Waves Appl.*, vol. 31, no. 18, pp. 2036–2045, Dec. 2017.
[37] K.-L. Wu, C. Wei, X. Mei, and Z.-Y. Zhang, "Array-antenna decoupling surface," *IEEE Trans. Antennas Propag.*, vol. 65, no. 12, pp. 6728–6738, Dec. 2017.
[38] Z. Niu, H. Zhang, Q. Chen, and T. Zhong, "Isolation enhancement in closely coupled dual-band MIMO patch antennas," *IEEE Antennas Wireless Propag. Lett.*, vol. 18, no. 8, pp. 1686–1690, Aug. 2019.
[39] X. Shen, Y. Liu, L. Zhao, G.-L. Huang, X. Shi, and Q. Huang, "A miniaturized microstrip antenna array at 5G millimeter-wave band," *IEEE Antennas Wireless Propag. Lett.*, vol. 18, no. 8, pp. 1671–1675, Aug. 2019.

ZIYANG WANG (Member, IEEE) was born in Henan, China, in 1991. He received the Ph.D. degree in electromagnetic wave and microwave technology from Xidian University, Xi'an, China, in 2018. He is currently a Postdoctoral Researcher with the Department of Electronic Engineering, Tsinghua University. His research interests include 1-bit element design, phase controlled electromagnetic surface, vortex electromagnetic wave and spatial beamforming design, global optimization algorithm, 5G MIMO antenna, array antenna decoupling, and antenna broadband design.

CHENGLEI LI (Student Member, IEEE) received the B.S. degree from the University of Electronic and Science Technology of China, Chengdu, China, in 2007. He is currently pursuing the M.S. degree with the Department of Electronic Engineering, Tsinghua University, Beijing, China. His current research interests include isoflux beamforming technology, genetic algorithm in electromagnetics, and reconfigurable reflectarray antenna.

YINGZENG YIN (Member, IEEE) received the B.S., M.S., and Ph.D. degrees in electromagnetic wave and microwave technology from Xidian University, Xi'an, China, in 1987, 1990, and 2002, respectively. From 1990 to 1992, he was a Research Assistant and an Instructor with the Institute of Antennas and Electromagnetic Scattering, Xidian University. From 1992 to 1996, he was an Associate Professor with the Department of Electromagnetic Engineering, Xidian University. Since 2004, he has been a Professor with Xidian University. His research interests include design of microstrip antennas, artificial magnetic conductors, phased array antennas, and computer aided design for antennas.